Supplementary Information for:

Emulating Photosynthetic Processes With Light Harvesting Synthetic Protein (Maquette) Assemblies on Titanium Dioxide

Christopher J. Hobbs,[a] Nicholas Roach,[a] Pawel Wagner,[a] Holly van der Salm,[b] Jonathan E. Barnsley,[b] Keith C. Gordon,[b] Goutham Kodali,[c] Christopher C. Moser,[c] P. Leslie Dutton,[c] Klaudia Wagner*[a] and David L. Officer*[a]

[a]The ARC Centre of Excellence for Electromaterials Science and the Intelligent Polymer Research Institute, University of Wollongong, NSW 2522, Australia
[b]University of Otago, Department of Chemistry, Dunedin 9016, New Zealand
[c]The Johnson Research Foundation and Department of Biochemistry and Biophysics, University of Pennsylvania, Philadelphia, PA 10104, USA

*email: kwagner@uow.edu.au; davido@uow.edu.au

Table of Contents

1. Materials

The reagents N-cyclohexyl-2-aminoethansulfonic acid (CHES; Sigma-Aldrich), potassium chloride (KCl; Sigma-Aldrich), potassium hydroxide (KOH; Sigma-Aldrich), tetrabutylammonium perchlorate (TBAP; Sigma-Aldrich), 4-*tetr*-butylpyridine (tBP; Sigma-Aldrich), 1-butyl-3-methylimidazolium iodide (BMII; Sigma-Aldrich), lithium iodide (LiI; Sigma-Aldrich), and iodine (I_2; Merck) were all purchased reagent grade and used without further treatment. Dimethyl sulfoxide (DMSO; Sigma-Aldrich), hydrochloric acid (HCl; Sigma-Aldrich), anhydrous valeronitrile (VN; Sigma-Aldrich), anhydrous acetonitrile (ACN; Sigma-Aldrich), and anhydrous tetrahydrofuran (THF; Sigma-Aldrich) were all purchased and used without further purification.

Fluorine-doped tin oxide (FTO) coated glass (Hartford TEC8, 2.3 mm, *R*s ≤8 ohms/square) was used for conductive substrates. Transparent (DSL 18 NR-T TiO_2 paste, Dyesol) titanium dioxide (TiO_2) layers were screen printed onto the FTO coated substrate to obtain varying thicknesses.

Porphyrin

5,10,15-Tri[4-carboxyphenyl)-5-phenylporphyrinato zinc (II) (ZnTCPP) was prepared as previously reported.[1]

Maquette expression

Codon optimised synthetic genes were obtained from DNA2.0 in PJ414 vector. The protein was expressed with a histidine tag in E. coli BL21 (DE3) cells for 5 hours at 37 °C, after induction with isopropyl-thiogalactopyranoside (IPTG) (0.5 mM).[2] The cells were harvested by centrifugation, resuspended in KH_2PO_4 buffer with octylthioglucoside (1%), and lysed by sonication with a micro-tip attachment. Lysate was centrifuged at 25,000 g for 25 minutes, with supernatant applied to a Ni nitrilotriacetic acid superflow resin (Qiagen) on an Akta FPLC. The His-tag was cleaved by recombinant tobacco etch virus N1a protease overnight, and final purification was via Waters reverse-phase HPLC. Molecular weight was assayed by either MALDI or ESI mass spectrometry.[3]

2. Instrumentation and Characterisation

Current-voltage curves of devices under simulated 100 mW.cm^{-2} AM 1.5 illumination (Oriel) were recorded in a voltage range from -0.25 to 0.85 V using a Keithley 2400 digital sourcemeter after calibration using a certified Si diode quipped with a KG5 filter (Pecell). The device area was masked with black paint.

Incident photon-to-current conversion efficiency (IPCE) was recorded using a QEX10 quantum efficiency measurement system (PV measurements). The light was focused onto a single point (smaller than the active area). DC mode was chosen for both calibration and measurements. The photocurrent responses of the devices were recorded in 1 nm wavelength steps. The measured currents were referenced to a calibrated Si diode (THORLABS LMR1/M).

Electrochemical impedance spectroscopy (EIS) measurements were recorded using a Gamry Reference 600 instrument (Garry Instruments, Warminster, PA). These were done while illuminating the DSSC devices with 100 mW cm^{-2} using a calibrated AM 1.5 illumination at open-circuit conditions between 0.1 Hz and 100 kHz with an AC amplitude of 10 mV. Spectra were analysed and fitted using ZView2 with the equivalent circuit shown in Fig. 4c.

The electrochemical data was obtained using square wave voltammetry in anhydrous acetonitrile containing 0.1 M tetrabutylammonium perchlorate (TBAP) as supporting electrolyte. The working electrodes were 700 nm TiO_2 printed FTO slides with ZnTCPP sensitised from THF, bound from CHES buffer, and purified maquette-ZnTCPP ensemble. Solutions were degassed prior to measurements and ferrocene was added as an internal reference. Conversion to NHE potentials was achieved using

$$E_{1/2}(\text{NHE}) = E_{1/2}(\text{Ag/Ag}^+) - E_{1/2}(\text{Fc/Fc}^+) + 0.63\ \text{V}$$

where 0.63 V is the Fc/Fc$^+$potential in acetonitrile versus NHE.[4]

Pt mech and Ag/Ag$^+$ electrodes were used as the counter and quasi-reference electrode respectively. The results were recorded using an eDAQ potentiostat system controlled by eDAQ EChem software.

Absorbance spectra were all recorded using a Shimadzu UV-1800 spectrophotometer.

3. Supplementary Methods

Stability in CHES buffer

Stability of the absorbance spectra from a mixture maquette and ZnTCPP was assessed with 5 µM maquette in CHES buffer mixed via pipette action for 10 sec with 2 µM ZnTCPP from a stock 1 mM DMSO solution in a quartz cuvette. Absorbance (include 0 min) was measured every 5 min using a Shimadzu UV-1800 spectrophotometer with no further disturbance of the measured solution nor cuvette. Similarly, the stability of ZnTCPP in CHES buffer was assessed by mixing 2 µM ZnTCPP in CHES buffer via pipette action for 10 sec with ZnTCPP from a stock 1 mM DMSO solution in a quartz cuvette. Absorbance (include 0 min) was measured every 5 min using a Shimadzu UV-1800 spectrophotometer with no further disturbance of the measured solution or cuvette.

Resonance Raman spectroscopy

Resonance Raman spectra were collected using a setup that has been previously described.[5] In short, it is composed of an excitation beam and collection lens in a 135° backscattering arrangement. Scattered photons were focused on the entrance slit of an Acton SpectraPro500i spectrograph with a 1200 grooves/mm grating, which disperses the radiation in a horizontal plane on a Princeton Instruments Spec10 liquid-nitrogen-cooled CCD detector. A solid-state CrystaLaser was used for 448.0 nm excitation wavelength and a notch filter (Kaiser Optical, Inc.) matched to this wavelength was used to remove the laser excitation line.

Samples were all measured in CHES buffer, with a maquette concentration of 20 µM. Porphyrin concentration in CHES buffer alone was 20 µM, and 10, 20, 30 µM when mixed with maquette to produce intended ratios. Porphyrin samples were diluted from a stock solution of 1 mM in DMSO.

Metalloporphyrin vibrational modes are known to show considerable sensitivity to the environment, whether in regards to planarity, metal oxidation state/spin or the presence of an auxillary moiety.[6-10] The resonance Raman solution spectra of the spectroscopic changes for ZnTCPP "core size" marker bands with the addition of the GL-maquette are shown in Fig. S1 and are analogous to those previously reported for other maquettes.[1] Relative intensities for bands within 890-1610 cm^{-1} range increase when compared to the bands at 678 and 714 cm^{-1}. Relative band intensities for ν4 and ν29 (1339-1353 cm^{-1}) also change, with ν29 increasing by over 20%. There is a small red shift of this ν29 band from 1353 to 1350 cm^{-1}. At the lower energy region, there is a small blue shift of the 1003 cm^{-1} band (ν15) to 1006cm^{-1}. The resonance Raman data shown serves as supporting evidence that porphyrin structural changes

have occurred, which is a result of binding of the porphyrin to the maquette through a histidine residue. Feitelson & Spiro have shown that low frequency (150-250 cm^{-1}) resonance Raman data is strong evidence for the Zn-histidine stretch, however, within obtained data in the low frequency regions, determination of the highly informative Zn-histidine mode is unlikely due to the desolate nature of the data.[11]

Isolation of maquette-ZnTCPP ensembles

Isolation and concentration of a solution containing maquette-ZnTCPP was undertaken using a protein concentrator tube (3 kDa MWCO, Amicon Ultra-4 centrifugal filter; Sigma-Aldrich), with the solution subjected to multiple cycles. CHES buffer containing 40 and 100 µM maquette and ZnTCPP (from a 2 mM ZnTCPP in DMSO stock solution) respectively was mixed for 1 h to ensure complete binding and saturation of maquette binding sites (whereby the maquette has 2 Zn porphyrin binding sites). Mixture was subjected to 5 centrifugal cycles of 12,000 rpm for 20 min, with the mixture CHES buffer added to the filter so that the total volume was ~2 mL between cycles. Absorbance of a 100-fold dilution of the final concentrated solution in CHES buffer after 5 centrifugal cycles was measured.

Determination of the stoichiometric relationship of isolated maquette-ZnTCPP ensembles

Calculation of the stoichiometric relationship from an isolated maquette-ZnTCPP solution (Fig. 2b) was determined using the relationship between absorbance at 280 nm (absorbance peak for maquettes), and the Soret peak of ligated ZnTCPP. However, as ligated ZnTCPP has a small influence in absorbance at 280 nm, the relative amount of influence was first determined. Fig. S3 displays the relative rise in absorbance of the ligated (within maquette) ZnTCPP Soret peak compared to the increase at 280 nm in CHES buffer, with the resulting gradient shown. Increases in absorbances were recorded with excess maquette present, ensuring that a negligible increase in absorbance was obtained from the non-ligated ZnTCPP. The gradient was determined to be 28.1 ±0.48, representing the relative increase in absorbance at the ligated Soret peak compared to the increase at 280 nm. Therefore, with the extinction coefficient known for ligated ZnTCPP (within the maquette), concentrations of both ligated ZnTCPP and also the GL-maquette could be calculated from an isolated solution containing maquette-ZnTCPP ensembles according to Equation S1.

A 100-fold diluted sample in CHES buffer of the isolated maquette-ZnTCPP mixture was measured (Fig. 2b), with the peak at 433 nm corresponding to ligated ZnTCPP within the maquette. With the influence of ligated ZnTCPP on absorbance at 280 nm previously

determined, the maquette and ligated ZnTCPP concentrations were calculated (Equation S1) from the absorbance of the diluted sample, giving a ratio of 1:1.95, maquette to porphyrin respectively.

[maquette] = (A_p – (S_p/R)) / ε_M **Equation S1**

where A_p = measured absorbance at 280 nm, S_P = measured absorbance at Soret peak of ligated porphyrin, R = ratio of ligated Soret peak to maquette absorbance, ε_M = extinction coefficient of the maquette at 280 nm (being 11,200 M^{-1} cm^{-1}).

Desorption from TiO_2.

Quantification of porphyrin from treated TiO_2 was determined by desorption via submerging the TiO_2 samples in 3 ml of 2 M HCl / THF. Samples were sealed and kept in the dark at RT for 48 h, before the UV.vis. absorbance was measured for each resulting solution. The measured absorbance was compared to a standard curve known concentrations of porphyrin in 2 M HCl / THF as to ascertain the concentration of porphyrin present on each electrode.

Stability in CHES buffer

To analyse the stability of ZnTCPP in aqueous CHES buffer, either ligated to the maquette, or free in solution, time-based absorbance spectra were recorded. Excess maquette was mixed with ZnTCPP in CHES buffer, with the UV-Vis. absorbance measured every 5 mins for 1 hour (Fig. S1). No spectral changes occurred over time, indicating that ZnTCPP binds quickly to the maquette, and that the ensemble is stable in CHES buffer. In contrast, the stability of ZnTCPP in CHES buffer was analysed. ZnTCPP UV-Vis. absorbance was measured every 5 mins for 1 hour in aqueous CHES buffer (Fig. S2). Similar to the result with the ensemble, no spectral changes were observed over time, indicating that ZnTCPP is stable in aqueous CHES buffer.

Determination of ideal binding conditions of ensembles to TiO_2

Binding to TiO_2 was undertaken using the isolated maquette-ZnTCPP solution (Fig. S2), with initial binding studies performed to determine ideal concentrations and binding exposure times. Two different thicknesses of TiO_2 (2.5 and 12.5 µm) was used in the time-exposure studies for maquette binding, exposed to the isolated ensemble solution. The isolated ensemble solution was diluted to a concentration of 80 µM ligated ZnTCPP (and subsequently 41 µM maquette),

with 100 µl drop-casted onto TiO_2 samples. Substrate samples were placed in a petr-dish, sealed with parafilm, and left in a fridge (at 4 ^oC) for time variables. Following exposure time, substrates were rinsed by submersion in CHES buffer and dried via N_2 gas stream before measurements. Fig. S4a shows that on the 2.5 µm films, the maquette-ZnTCPP ensembles saturate the substrate by 6 h, with no additional binding from increased exposure times. Of note is that the absorbance spectra of all substrates after the variable exposure times are identical, indicating a stable surface of bound ensemble. As the Soret peak region on the thicker TiO_2 was too intense, the Q-band region was used for analysis of ensemble binding to the substrate (Fig. S4 inset). It was apparent that the thicker film needed a longer exposure time for binding saturation of the substrate (>24 h, Fig. S4b) compared to the thinner film used. This is likely due to the protein needing additional time to manoeuvre through the additional layers of pores in the thicker TiO_2.

A concentration dependent binding study to 2.5 µm TiO_2 was undertaken for determination of an ideal maquette concentration to use for saturation of the substrate. A ratio of 1:1 maquette to ZnTCPP was used to keep the absorbance of the Soret peak region within a measurable range and to also ensure complete ligation of ZnTCPP within the maquette. A CHES buffer solution of appropriate concentration was drop-casted (100 µl) onto the TiO_2 sample substrates. Samples were then placed in a petr-dish, sealed with parafilm, and left in a fridge (at 4 °C) for 48h. Following exposure time, substrates were rinsed by submersion in CHES buffer and dried via N_2 gas stream before measurements. As shown in Fig. S5, no significant increase in the absorbance of the Soret peak is apparent (within standard deviation) when concentrations of ≥20 µM (ligated ZnTCPP) is used. As a 1:1 ratio was used, the results indicate that using a maquette concentration of ≥20 µM for an exposure time of 48 h is sufficient for saturation of the substrate surface.

Determination of HOMO-LUMO energy levels of the TiO_2 bound porphyrins

To determine if the electronic state of ZnTCPP was aligned appropriately for redox coupling within a device, the HOMO-LUMO energy levels of the porphyrins were evaluated. The electrochemical determination of the oxidation potential of ZnTCPP (the electroactive material) in each of the modified TiO_2 electrodes (for calculation of the HOMO) was determined congruently with the optical band gap (E_{opt}) onset at the higher wavelength from the absorption spectra (Figure 3D) in order to calculate the LUMO level ($E_{LUMO} = E_{HOMO} – E_{opt}$). The calculated HOMO-LUMO levels would indicate if each of the ZnTCPPs were suitable for regeneration with the redox couple (HOMO level) and could undergo electron

injection processes into the conduction band (CB) of TiO_2 (LUMO level). To evaluate HOMO values, electrochemistry of the modified TiO_2 electrodes were studied through square wave voltammetry (Figure S6).

Modified 0.7 μm TiO_2 samples were prepared using ZnTCPP in THF, ZnTCPP salt in CHES buffer, and maquette-ZnTCPP ensemble in CHES buffer. Square wave voltammetry was employed to analyse the half-wave potentials ($E_{1/2}$) of the first oxidation peak. This was done by using a 3 electrode cell with the modified TiO_2 electrode as working electrode, platinum mesh as a counter electrode, Ag/Ag^+ as a reference and 0.1 M tert-butylammonium perchlorate (TBAP) in acetonitrile as electrolyte.

For an unmodified TiO_2 electrode, no significant peaks were observed at applied potentials of 0.5 – 1.3 V (vs NHE). In contrast, a substantial peak at 0.91 V (vs NHE) was evident for the ZnTCPP sensitised TiO_2 electrode (blue line, Fig. S6). This peak was assigned to the $E_{1/2}$ of the first oxidation for ZnTCPP bound to TiO_2. Similarly, when ZnTCPP is bound to TiO_2 from CHES buffer, a peak at 0.91 V (vs NHE) was observed (red line, Fig. S6), assigned to the $E_{1/2}$ of the first oxidation. This indicated that the electronic state of ZnTCPP had not changed despite the difference in binding modes. The significantly lower current observed for the carboxylate ZnTCPP on TiO_2 was due to the aggregative effects hindering electron injection into the electrode (as evident from the absorption spectrum (red line, Fig. 3d). For the GL-maquette-ZnTCPP TiO_2 electrode, a peak at 0.89 V (vs NHE) assigned to the $E_{1/2}$ of the first oxidation was apparent (green line, Fig. S6). This is ~20 mV different from the other bound porphyrins, and is likely due to a change in the electronic state of ZnTCPP as a result of ligation to the maquette through its central zinc. The lower current-response for GL-maquette-ZnTCPP compared to the sensitised ZnTCPP was attributed to the significantly lower concentration of ZnTCPP present (2.30 ± 0.01 compared to 13.54 ± 0.52 nanomol cm^{-2} μm^{-1}, respectively, Table 1).

4. Supplementary Figures and Tables

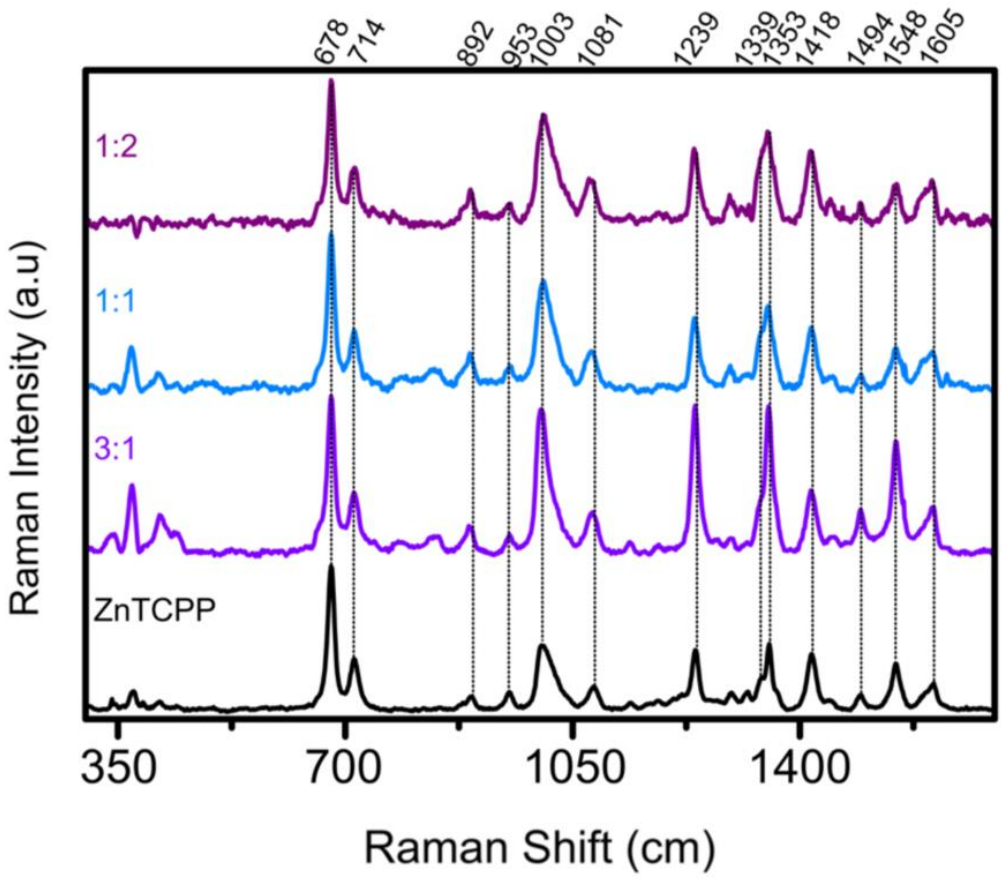

Figure S1. Resonance Raman spectra in CHES buffer of the bound ZnTCPP in the GL-maquette. Resonance Raman data of solution of ZnTCPP and maquette in ratios of 3:1 (violet spectrum), 1:1 (blue spectrum) and 1:2 (purple spectrum). The ZnTCPP spectrum is also shown (black spectrum). Spectra were collected at an excitation wavelength of 448 nm in CHES buffer.

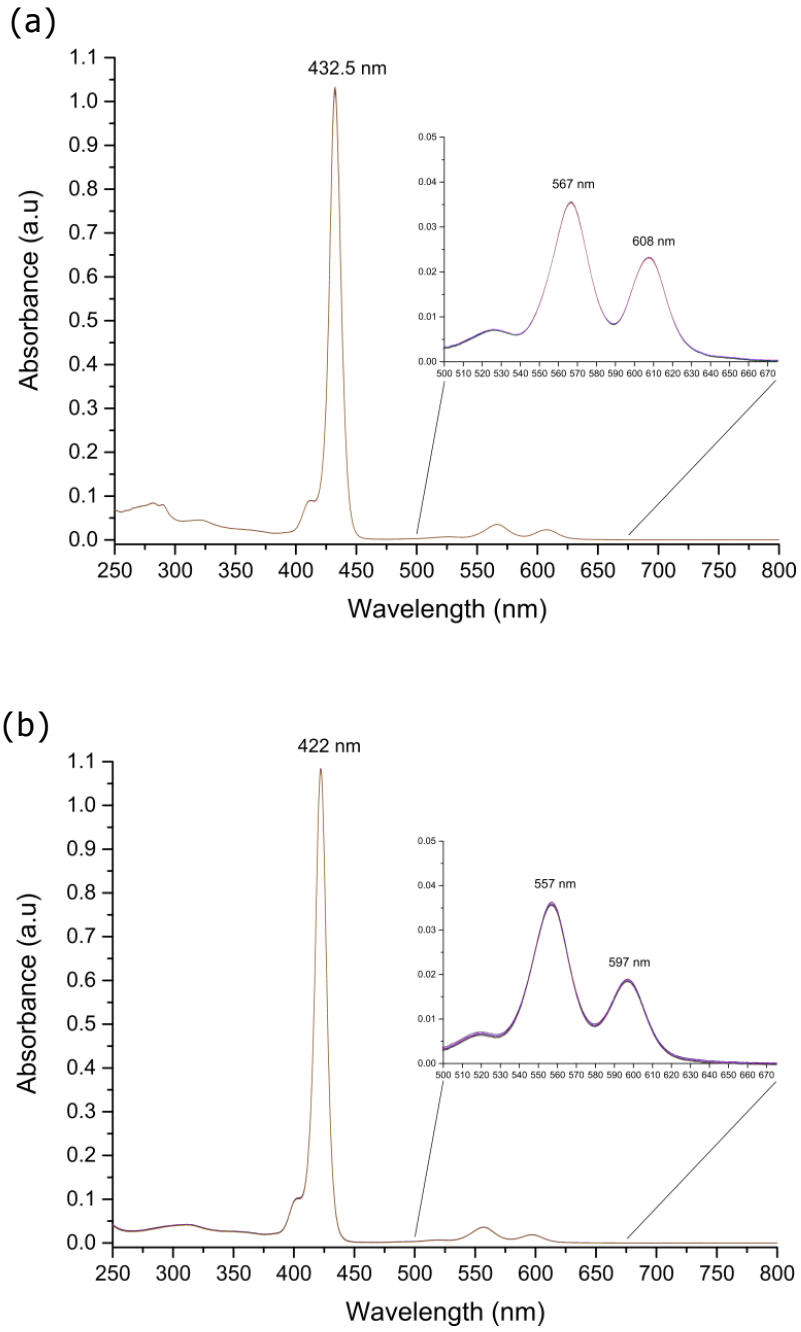

Figure S2. Stability in CHES buffer of the bound ZnTCPP in the GL-maquette. (a) UV- vis spectra of a solution of 5 μM maquette and 2 μM ZnTCPP in CHES buffer. (b) UV- vis spectra of a solution of 2 μM ZnTCPP in CHES buffer. Absorbance was measured every 5 mins over a period of 1 h for both samples.

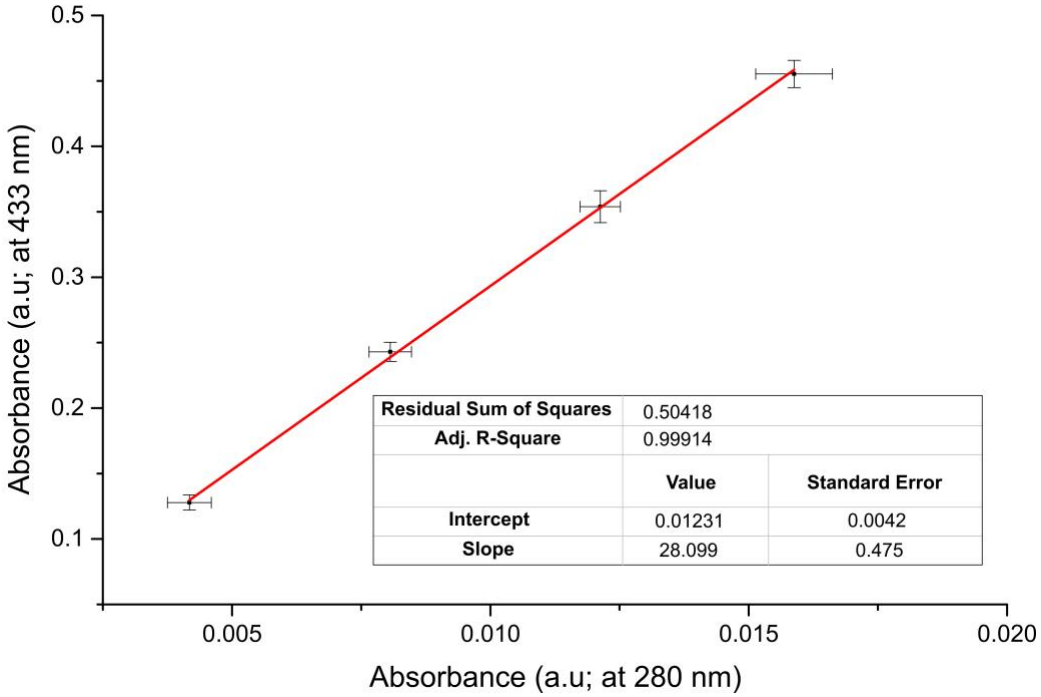

Figure S3. Determination of the relationship between the increase in absorbance at 280 nm and 433 nm. A plot of the increase in absorbance at 280 nm compared to increases at 433 nm when ZnTCPP is added to a solution of maquette. Based on the resulting gradient, an arbitrary increase in absorbance at 280 nm results in a 28.1 fold increase in the absorbance at 433 nm (n=4, ± standard deviations).

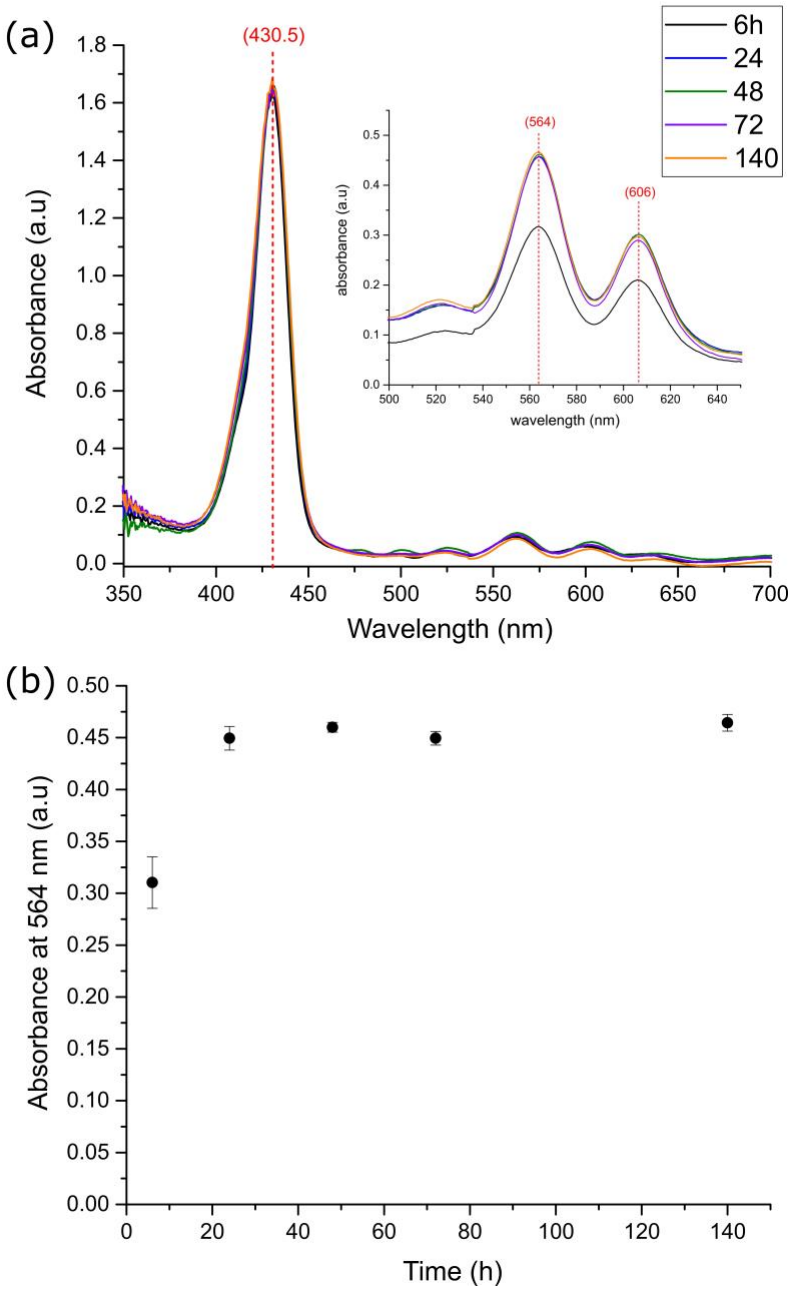

Figure S4. Absorbance of GL-maquette-ZnTCPP on TiO_2 from aqueous buffer over time. (a) 2.5 μm TiO_2 exposed to purified GL-maquette-ZnTCPP ensembles (1:1.95) in aqueous buffer, with inset showing Q- band region from 12.5 μm TiO_2. (b) Absorbance changes over time at 564 nm from 12.5 μm TiO_2 exposed to purified GL-maquette-ZnTCPP ensembles (1:1.95) in aqueous buffer. Averages shown with standard deviations, where n=4.

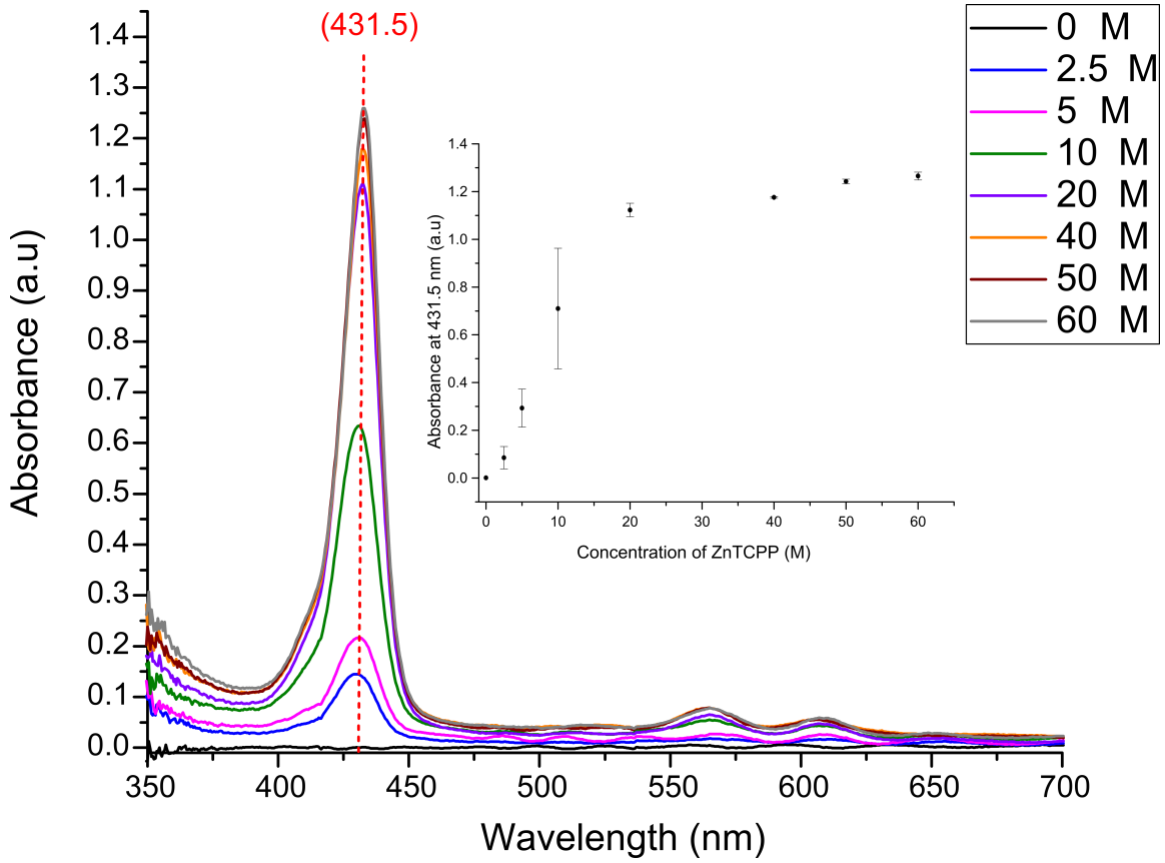

Figure S5. Absorbance of TiO_2 bound with increasing concentrations of 1:1 GL-maquette:ZnTCPP ensembles. 2.5 μm TiO_2 was exposed to increasing concentrations over 48 h of GL-maquette-ZnTCPP ensembles from aqueous buffer in a ratio of 1:1, with the inset showing the increase in the observed Soret peak at 431.5 nm. Averages shown with standard deviations, where n=4.

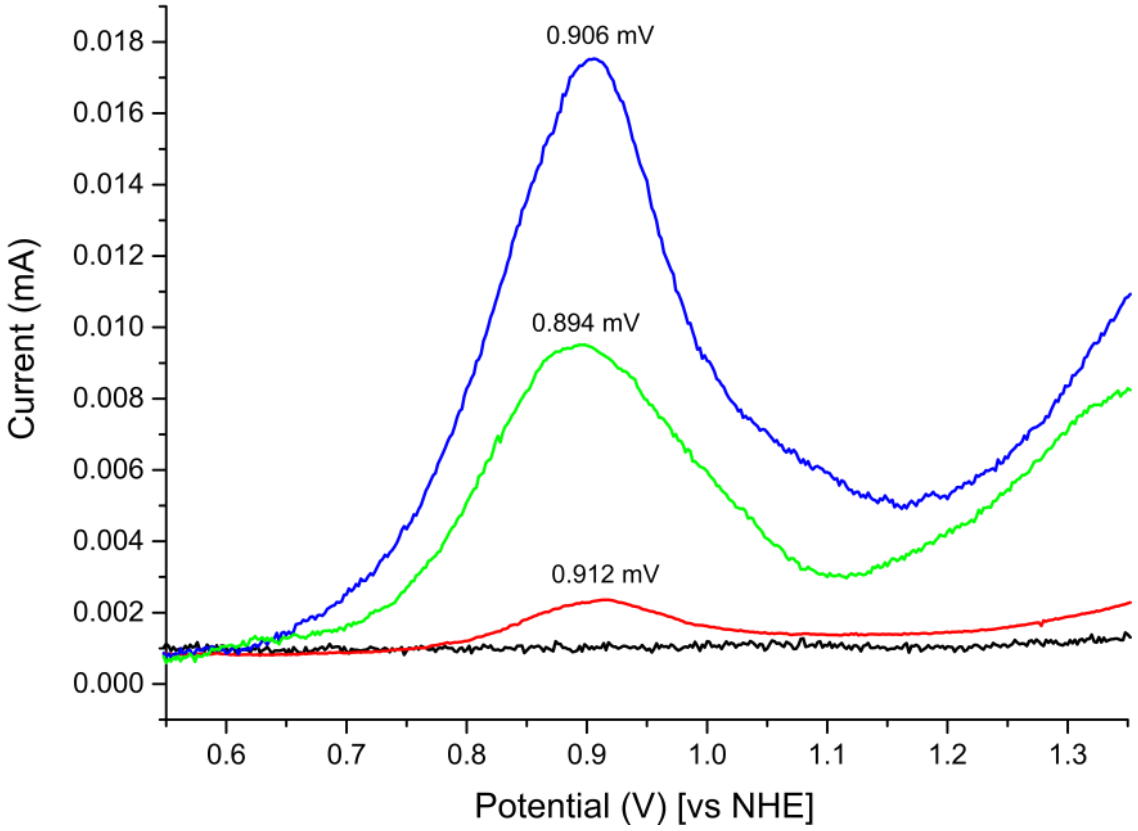

Figure S6. Square-wave voltammetry of 0.7 μm modified TiO_2 in 0.1M TBAP acetonitrile. First oxidation peaks of TiO_2 surfaces modified with ZnTCPP sensitised from THF (blue line), the carboxylate salt of ZnTCPP bound from CHES buffer (red line), and GL-maquette-ZnTCPP ensemble from CHES buffer (green line). The unmodified TiO2 background scan (black line) is also shown. Scan rate: 20 mV s^{-1}.

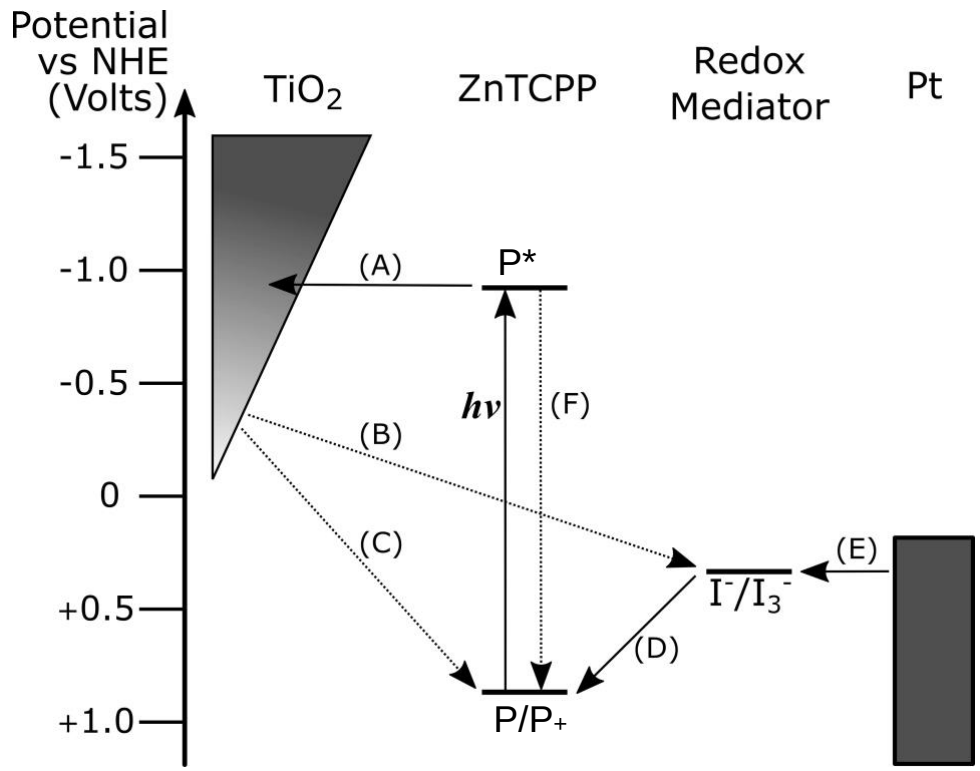

Figure S7. Energy level diagram for maquette-based photovoltaic device. Energy level diagram for photovoltaic device with GL-maquette-ZnTCPP (P) ensemble immobilised on TiO_2, with depiction of the various photophysical pathways. (A) electron injection from excited ZnTCPP (P*), (B) electron recombination with redox mediator, (C) electron recombination with ZnTCPP cations (P^+), (D) regeneration of ZnTCPP cations (P^+) by redox mediator, (E) recycling of redox mediator at counter electrode, and (F) relaxation of the ZnTCPP photoexcited state ($P^+ \rightarrow P$).

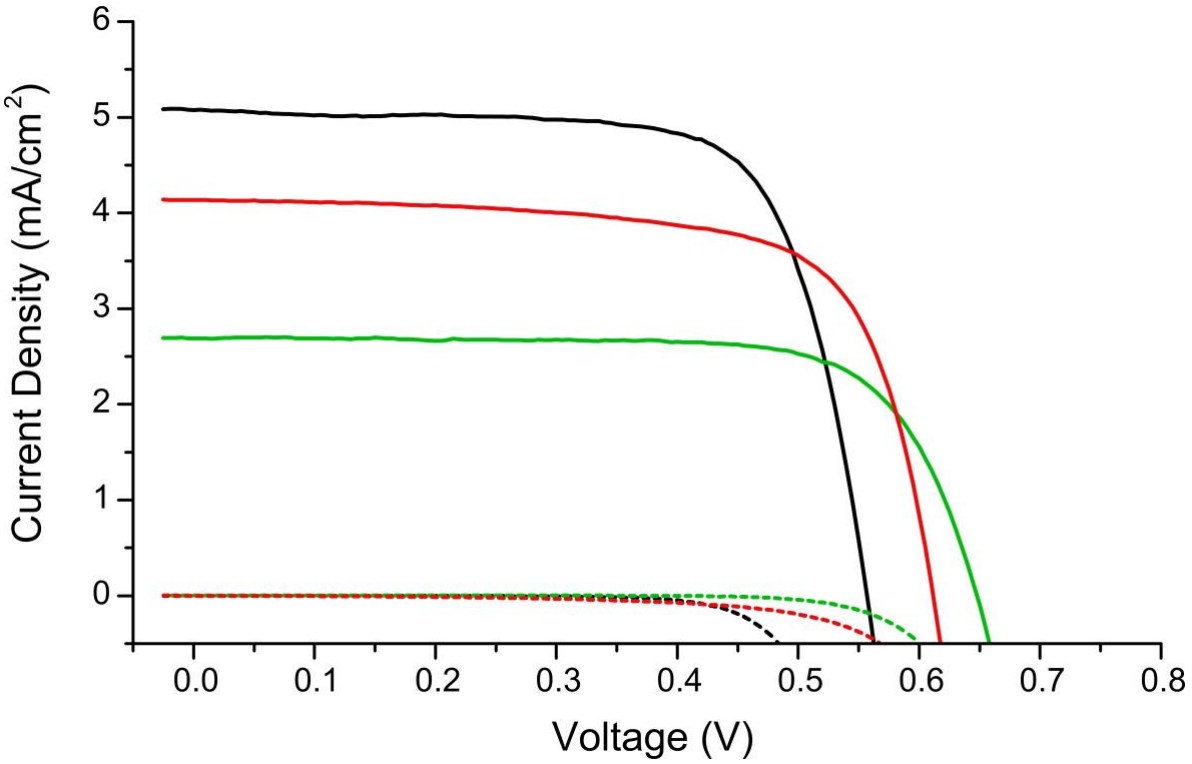

Figure S8. Current density (*J*) versus voltage (*V*) curves for photovoltaic devices using 2.5 µm TiO_2. *JV* curves for illuminated devices are solid lines and in the dark are dotted lines for immobilised GL-maquette-ZnTCPP ensemble from CHES buffer (green lines), bound carboxylate salt of ZnTCPP from CHES buffer (red lines), and sensitised ZnTCPP from THF (black lines).

Table S1. UV-Vis. absorbance peak positions and extinction co-efficients (ε) of ZnTCPP in DMSO, in DMSO/CHES buffer and ZnTCPP/maquette in DMSO/CHES buffer after 1 h equilibration. Data for ZnTCPP with maquette in CHES buffer determined from binding titration, with peaks determined where maquette was in excess.

Solution	Soret Peak (nm)	ε at Soret Peak (M^{-1} cm^{-1})	Q-band positions (nm)
ZnTCPP/DMSO	429.5	514,600	562, 601
ZnTCPP/DMSO/CHES buffer	422	478,000	557, 597
ZnTCPP/Maquette/DMSO /CHES buffer	433	476,000	567, 608

Table S2. UV-Vis. absorbance peak positions of ZnTCPP covalently bound, electrostatically bound and maquette bound to dry films of TiO_2.

Sample	Soret Peak (nm)	Q-band Positions (nm)
ZnTCPP	426	558.5, 599
From CHES buffer	405.5, 425	560.5, 602
From CHES buffer ligated with maquette	432.5	565, 607.5

Table S3. Electrochemical impedance spectroscopy (EIS) determined resistances (R) and capacitances (C). Resistance, capacitance, and electron lifetime measurements (Table 1) were obtained by fitting an equivalent circuit (Fig. 4c) to the EIS data obtained at *Voc* and 100 mW cm^{-2} simulated at AM 1.5 sunlight illumination. Estimated errors for each EIS parameter as determined by the fitted algorithm are shown.

	R_s (Ω)	R_1 (Ω)	C_1 (10^{-6} F)	R_2 (Ω)	C_2 (10^{-5} F)
Sensitised Porphyrin	6.0 (± 0.10)	8.7 (± 0.29)	2.26 (± 0.10)	35.3 (± 0.79)	2.24 (± 0.09)
Porphyrin Salt	5.5 (± 0.11)	7.7 (± 0.24)	2.40 (± 0.13)	32.0 (± 0.80)	4.50 (± 0.18)
Immobilised Ensemble	5.5 (± 0.10)	4.5 (± 0.14)	2.60 (± 0.19)	113 (± 1.6)	7.12 (± 0.11)

5. References

1. G. Kodali, J. A. Mancini, L. A. Solomon, T. V. Episova, N. Roach, C. J. Hobbs, P. Wagner, O. A. Mass, K. Aravindu, J. E. Barnsley, K. C. Gordon, D. L. Officer, P. L. Dutton and C. C. Moser, *Chem. Sci.*, 2017, **8**, 316-324.
2. D. Robertson, R. Farid, C. C. Moser, J. Urnauer, S. Mulholland, R. Pidikiti, J. Lear, J. Wand, W. Degrado and P. L. Dutton, *Nature*, 1994, **368**, 425-432.
3. T. A. Farid, G. Kodali, L. A. Solomon, B. R. Lichtenstein, M. M. Sheehan, B. A. Fry, C. Bialas, N. M. Ennist, J. A. Siedlecki, Z. Zhao, M. A. Stetz, K. G. Valentine, J. L. R. Anderson, A. J. Wand, B. M. Discher, C. C. Moser and P. L. Dutton, *Nat. Chem. Biol.*, 2013, **9**, 826.
4. V. V. Pavlishchuk and A. W. Addison, *Inorg. Chim. Acta*, 2000, **298**, 97-102.
5. R. Horvath and K. C. Gordon, *Coord. Chem. Rev.*, 2010, **254**, 2505-2518.
6. J. A. Shelnutt, K. Alston, J. Y. Ho, N. T. Yu, T. Yamamoto and J. M. Rifkind, *Biochemistry*, 1986, **25**, 620-627.
7. J. A. Shelnutt, C. J. Medforth, M. D. Berber, K. M. Barkigia and K. M. Smith, *J. Am. Chem. Soc.*, 1991, **113**, 4077-4087.
8. T. G. Spiro, J. D. Stong and P. Stein, *J. Am. Chem. Soc.*, 1979, **101**, 2648-2655.
9. T. G. Spiro and T. C. Strekas, *J. Am. Chem. Soc.*, 1974, **96**, 338-345.
10. Y.-H. Zhang, W. Zhao, P. Jiang, L.-J. Zhang, T. Zhang and J. Wang, *Spectrochim. Acta, Part A*, 2010, **75**, 880-890.
11. J. Feitelson and T. G. Spiro, *Inorg. Chem.*, 1986, **25**, 861-865.